applied optics

Thermally induced phase mismatching in a repetitively Gaussian pulsed pumping KTP crystal: a spatiotemporal treatment

Mostafa Mohammad Rezaee,[1] Mohammad Sabaeian,[1,*] Alireza Motazedian,[1] Fatemeh Sedaghat Jalil-Abadi,[1] Hadi Askari,[2] and Iman Khazrk[3]

[1]Department of Physics, Faculty of Science, Shahid Chamran University of Ahvaz, Ahvaz, Iran
[2]Department of Physics, Faculty of Science, University of Isfahan, Isfahan, Iran
[3]Department of Physics, Faculty of Basic Science, Arak University, Arak, Iran
*Corresponding author: sabaeian@scu.ac.ir

Received 6 April 2015; accepted 19 April 2015; posted 23 April 2015 (Doc. ID 237571); published 15 May 2015

Thermally induced phase mismatching (TIPM) has been proven to be an influential issue in nonlinear phenomena. It occurs when refractive indices of crystal are changed due to temperature rise. In this work, the authors report on a modeling of spatiotemporal dependence of TIPM in a repetitively pulsed pumping KTP crystal. Gaussian profiles for both spatial and temporal dependences of pump beam were used to generate second-harmonic waves in a type II configuration. This modeling is of importance in predicting the nonlinear conversion efficiency of crystals when heat is loaded in the system. To this end, at first, an approach to solve the heat equation in a repetitively pulsed pumping system with consideration of the temperature dependence of thermal conductivity and realistic cooling mechanisms such as conduction, convection, and radiation, is presented. The TIPM is then calculated through the use of experimental thermal dispersion relations of KTP crystal. The results show how accumulative behaviors of temperature and TIPM (with its reverse sign) happen when the number of pulses is increased. Fluctuations accompanying temperature and TIPM were observed which were attributed to the off-time between successive pulses. Moreover, in this work, a numerical procedure for solving a repetitively pulsed pumped crystal is introduced. This procedure enables us to solve the problem with home-used computing machines. © 2015 Optical Society of America

OCIS codes: (140.6810) Thermal effects; (190.0190) Nonlinear optics.

http://dx.doi.org/10.1364/AO.54.004781

1. INTRODUCTION

To generate new frequencies, nonlinear crystals must be exposed to intense laser radiations. As a side effect, heat is generated due to partial deposition of traveling wave energy in the crystal. This heat leads to so-called thermal effects which have been shown to be influential in degradation of the harmonic generation [1–3]. Among the various thermal effects, thermally induced phase mismatching (TIPM) has been proven to be a more critical issue compared to other harmful effects, such as thermal stresses and bulging [2–5]. There are several ways in which thermal effects can affect the performance of optical and laser systems. For example, in solid-state lasers, thermal depopulation happening through the Boltzmann's factor can reduce the output efficiency of laser [6]. Nonlinear lasers are affected mainly from the TIPM [2,3,7–9]. Thermal lensing (or dn/dT effect), which is a well-known effect, influences the beam quality of laser output and deviates the beam profile from its standard shape [10–12]. Thermal stresses that cause optical birefringence and bulging are of importance when depolarization loss and crystal fracture are of interest [13,14].

Recently, emerging two-dimensional (2D) materials, such as graphene, MoS_2, and topological insulators, have gained enormous interest due to their superior nonlinear optical properties [15–18]. These 2D materials possess large third-order nonlinearity and robust saturable absorption, enabling generation of broadband short pulses from microwave to optical frequencies [16,19]. Second-harmonic generation (SHG) from monolayer graphene has also been reported [20], having isotropic property. Nonetheless, when multilayer graphene is placed on a SiO_2/Si substrate, anisotropic SHG is observed [20]. For MoS_2, strong SHG for odd layer thickness has been observed, confirming noncentrosymmetric nature of odd layered MoS_2 2D crystal [21,22]. Despite amazing nonlinear optical properties of 2D materials, efficient or high-power SHG through these materials has not been reported yet. These may be due to the heat removal problem from such tiny

materials. Furthermore, heat problems in such 2D systems are a challenge still, since they have revealed exotic behavior leading to infinitively large intrinsic thermal conductivity [23–25]. For KTP crystal, the phase matching happens through the anisotropic property of KTP; however, for 2D materials this issue has not been inspected yet.

It should be noted that for commonly used crystals such as KTP or LBO, the TIPM happens only through the temperature change in refractive index (thermal dispersion) and this factor dominates other mechanisms, such as thermal stresses and bulging. Only for some new materials, such as oxyfluoride, the stress-optics effect can be influential [4]. For oxyfluoride, thermal dispersion is compensated by bulging having the same order of magnitude, but with an opposite sign, and therefore stresses control the thermal effects. For KTP crystal, due to the smallness of Young's modulus and thermal expansion coefficient by 2 and 1 order of magnitude, respectively, than those of oxyfluoride, thermal dispersion effects are greater significantly than thermal stresses and bulging. Therefore, this is responsible for TIPM in KTP.

The effect of TIPM in the SHG formalism for single-pass [3] and double-pass [2] continuous waves (CWs) using a numerical modeling has been studied and the effects of heat load on the second-harmonic waves (SHWs) have been revealed [9]. However, to the best of our knowledge, for a pulsed SHG, a precise calculation for TIPM has not been reported yet. This quantity is of great importance in determining the output efficiency of nonlinear lasers. The work of Regelskis *et al.* [26] is of interest in which they imposed an artificial temperature gradient to compensate for the TIPM for a pulsed system, but they did not show explicitly the TIPM due to the absorption of the fundamental wave (FW) and SHW, as Sabaeian and co-workers did it for CW operation [2,3]. Therefore, in this work we extract the behavior of TIPM for a pulsed pumped nonlinear crystal as a function of time and spatial coordinates. As the absorption of SHW is greater than that of FW by 8 times, we consider only the SHW absorption and this is the main source of heat generation [27,28].

In a pulsed system, the interaction length of nonlinear phenomena is small enough compared to crystal length, so that the nonlinear interaction can completely accomplish over a short length of the crystal. This means that the energy of the FW is transferred completely into the SHW [2,29]. In the CW regime, however, this event cannot occur thoroughly, since the crystal length is most often smaller than the interaction length. Therefore, the FW cannot give all its energy to the SHW.

Apart from this fact that in the present work, all parameters have been taken from experimental setups, a comprehensive model for temperature distribution and TIPM will be presented. We will consider a 3D numerical approach for temperature and TIPM in a KTP crystal under repetitively pumping configuration. For precise determination of TIPM, the temperature dependence of thermal conductivity as well as the realistic temperature boundary conditions of radiation and convention will be considered [28]. This would provide us with a precise insight into the problem. Inclusion of a mismatched phase (due to heat load in the crystal) in the field equations gives rise to a reduction in nonlinear conversion efficiency of SHG. To uncover this effect, a set of coupled equations for pulsed SHG should be solved (which is the future work of the author). This task has been done already for CW operation [2,3].

In this work, we demonstrate a general and numerical solution for time- and space-dependent TIPM equation for a repetitively pulse pumping configuration. We will also present an algorithm for numerical calculations that leads to a dramatic reduction in CPU time and RAM in cylindrical coordinates. To this end, homemade codes in finite difference time domain (FDTD) method have been written in Intel Fortran (ifort) 14.04 and run with Linux Ubuntu operating system. Without this contrivance, we were not able to solve this problem in a logical time with available processors and RAMs.

2. HEAT AND PHASE MISMATCHING EQUATIONS

The general form of heat equation governing the heat transport in solids is given by [27]

$$\rho C_p \frac{\partial T}{\partial t} - \nabla.(K(T) \cdot \nabla T) = S, \tag{1}$$

where T is the temperature, ρ ($= 2945$ kg/m^3 for KTP [30]) is the mass density, C_p ($= 728$ J/kg/K for KTP [31]) is the specific heat, $K(T)$ is a temperature-dependent thermal conductivity, and S is a heat source. As we are going to take the radiation as well as the convection into account and since the KTP thermal conductivity is a temperature-dependent quantity, a numerical method of the FDTD method is used for solving the heat equation. Discretization of Eq. (1) using $T(t, r, z) \rightarrow T(i, j, k)$ allows us to explore the temperature at any time of $t + \Delta t$ in terms of temperatures at time of t as [27]

$$\begin{aligned}
&T(i+1,j,k) \\
&= T(i,j,k) \\
&+ \frac{\Delta t}{\rho C_p} \frac{K(i,j+1,k) - K(i,j-1,k)}{2\Delta r} \frac{T(i,j+1,k) - T(i,j-1,k)}{2\Delta r} \\
&+ \frac{\Delta t}{\rho C_p} \frac{K(i,j,k+1) - K(i,j,k-1)}{2\Delta z} \frac{T(i,j,k+1) - T(i,j,k-1)}{2\Delta z} \\
&+ \frac{\Delta t}{\rho C_p} K(i,j,k) \frac{T(i,j+1,k) - T(i,j-1,k)}{2r\Delta r} \\
&+ \frac{\Delta t}{\rho C} K(i,j,k) \frac{T(i,j+1,k) - 2T(i,j,k) + T(i,j-1,k)}{\Delta r^2} \\
&+ \frac{\Delta t}{\rho C_p} K(i,j,k) \frac{T(i,j,k-1) - 2T(i,j,k) + T(i,j,k+1)}{\Delta z^2} \\
&+ \frac{\Delta t}{\rho C_p} S(i,j,k).
\end{aligned} \tag{2}$$

An experimental expression for thermal conductivity has been reported already and reads as [32–34]

$$K(T) = K_0 \times \frac{T_0}{T}, \tag{3}$$

where $K_0 = 13$ W/(mK) is the thermal conductivity of KTP at $T_0 = 298$ K [35].

The heat source term, S, suitable for a single pulse with Gaussian temporal and spatial profiles is given by [36]

$$S = PQ_0 \exp[-2(r/\omega_p)^2]\exp(-\alpha z)\exp[-(t/t_p)^2], \quad (4)$$

where ω_p(= 100 μm used in this work) is the beam spot size and $\alpha = 4\ \mathrm{m}^{-1}$ is the absorption coefficient of KTP at the SHW. $\tau_p = 50$ μs is the pulse duration. Note that in practice, the SHW grows exponentially with a very good approximation from the beginning face of the crystal. But, as seen in Eq. (4), we reversed it by convention, so that at $z = 0$ it has highest value and decays exponentially along the crystal axis.

In Eq. (4),

$$P = \int_{-\infty}^{+\infty} E_0 \exp[-(t/t_p)^2]\mathrm{d}t = E_0/(t_p\pi^{1/2}) \quad (5)$$

is the power of the pulse with $E_0 = 0.09$ J as the peak energy of the pulse. Q_0 is the normalization constant of spatial part, which is defined by [37]

$$Q_0 \int_0^{2\pi} \mathrm{d}\varphi \int_0^a e^{-2r^2/\omega_p^2} r\mathrm{d}r \int_0^l e^{-\alpha z}\mathrm{d}z = 1, \quad (6)$$

where l is the crystal length and a is the radius. The relation above leads to $Q_0 \simeq 2\alpha/\pi\omega_p^2$, where the assumption of $\exp(-\alpha l) \ll 1$ has been used [3,37].

The boundary condition of temperature with considering the conduction, convection, and radiation is given by [37]

$$-K(T)\mathbf{n}.\nabla T|_{\mathrm{boundary}} = h(T_W - T_\infty) + \sigma\varepsilon(T_W^4 - T_s^4)|_{\mathrm{boundary}}, \quad (7)$$

where $\hat{n}$ is an outward unit vector perpendicular to the surface. On beginning and end faces, Eq. (7) can be simplified to

$$\mp K(T)\frac{\partial T}{\partial z} = [h(T_W - T_\infty) + \sigma\varepsilon(T_W^4 - T_s^4)], \quad (8)$$

where − and + stand for the beginning and the end faces of the crystal, respectively; $h = 10\ \mathrm{Wm^{-2}\,K^{-1}}$ is the typical value of heat transfer coefficient reported in the literature [38]; $\sigma = 5.669 \times 10^{-8}\ \mathrm{Wm^{-2}\,K^{-4}}$ is the Stephan–Boltzman constant; $\varepsilon = 0.9$ is surface emissivity; T_∞, T_W, and T_s are the temperature of the fluid moving around the surface, temperature of the surface (wall), and ambient temperature, respectively.

In type II SHG, and for a negative biaxial crystal such as KTP, a temperature-dependent wave vector mismatching is given by [3]

$$\Delta k(T) = k^{o,\omega}(T) + k^{e,\omega}(T) - k^{e,2\omega}(T), \quad (9)$$

where $k^{o,\omega}(T) = n^{o,\omega}(T)\omega/C$, $k^{e,\omega}(T) = n^{e,\omega}(T)\omega/C$, and $k^{e,2\omega}(T) = n^{e,2\omega}(T)2\omega/C$ with $n^{o,\omega}$ and $n^{e,\omega}$ being the ordinary and extraordinary refractive indices at FW frequency, respectively, $n^{e,2\omega}$ being the extraordinary refractive index at the SHW frequency, and C being the speed of light. The TIPM is then calculated by [3]

$$\Delta\varphi = \int_0^z \Delta k(T)\mathrm{d}z' \quad (10)$$

In fact the temperature dependence of wave vector mismatching comes in refractive indices, that is, they change with temperature. They can be expanded around the ambient temperature as $\Delta n = n(T) - n_0 = (T - T_0)\partial n/\partial T$. This expansion should be applied on ordinary and extraordinary refractive indices that are not available at the moment. However, experimental principal refractive indices would help us to do that. The principal refractive indices as a function of wavelength, i.e., the dispersion relations, are given by Sellmeier expressions as [39]

$$n_X^2(\lambda, T_0) = 3.0065 + \frac{0.03901}{\lambda^2 - 0.04251} - 0.01327\lambda^2, \quad (11)$$

$$n_Y^2(\lambda, T_0) = 3.0333 + \frac{0.04154}{\lambda^2 - 0.04547} - 0.01408\lambda^2, \quad (12)$$

$$n_Z^2(\lambda, T_0) = 3.3134 + \frac{0.05694}{\lambda^2 - 0.05658} - 0.01682\lambda^2, \quad (13)$$

where wavelengths are in micrometers. The refractive index change coefficient, dn/dT, for KTP crystal have been given by experimental equations as follows [40]:

$$\frac{dn_X}{dT} = \left(\frac{0.1323}{\lambda^3} - \frac{0.4358}{\lambda^2} + \frac{1.2307}{\lambda} + 0.7709\right) \times 10^{-5}, \quad (14)$$

$$\frac{dn_Y}{dT} = \left(\frac{0.5014}{\lambda^3} - \frac{2.0030}{\lambda^2} + \frac{3.3016}{\lambda} + 0.7498\right) \times 10^{-5}, \quad (15)$$

$$\frac{dn_Z}{dT} = \left(\frac{0.3896}{\lambda^3} - \frac{1.3332}{\lambda^2} + \frac{2.2762}{\lambda} + 2.1151\right) \times 10^{-5}. \quad (16)$$

The ordinary and extraordinary refractive indices at which phase matching can be satisfied are calculated through the relation given below [40,41]:

$$n_\pm = \frac{\sqrt{2}}{\sqrt{-B \pm \sqrt{B^2 - 4D}}}, \quad (17)$$

where plus and minus signs stand for fast and slow light in the KTP crystal, respectively. Also, B and D are given by [40]

$$B = -\sin^2\theta\cos^2\varphi(b + c) - \sin^2\theta\sin^2\varphi(a + c) - \cos^2\theta(a + b), \quad (18)$$

$$D = -\sin^2\theta\cos^2\varphi(bc) - \sin^2\theta\sin^2\varphi(ac) - \cos^2\theta(ab), \quad (19)$$

where $a = n_X^{-2}$, $b = n_Y^{-2}$ and $c = n_Z^{-2}$. $\theta = 90°$ and $\varphi = 22.77°$ are the phase matching angles of KTP at $T = 298$ K [2]. For a fundamental wave wavelength of $\lambda = 1064$ nm and a SHW wavelength of 532 nm, and at $T = 298$ K, we have $n^{o,\omega} = 1.8296$, $n^{e,\omega} = 1.7466$, and $n^{e,2\omega} = 1.7881$ [42].

Therefore the TIPM, Eq. (10), can be calculated as

$$\Delta\varphi(z) = \int_0^z \frac{\omega}{c}[\Delta n^{o,\omega}(T) + \Delta n^{e,\omega}(T) - 2\Delta n^{e,2\omega}(T)]\mathrm{d}z', \quad (20)$$

which is better to transfer it to differential form as

$$\frac{d\varphi}{dz} = \frac{2\pi}{\lambda}[\Delta n^{o,\omega}(T) + \Delta n^{e,\omega}(T) - 2\Delta n^{e,2\omega}(T)], \quad (21)$$

where we have used $\lambda = 2\pi C/\omega$ as the fundamental wavelength.

Having found the temperature distribution in various times numerically, discretization of TIPM allows us to calculate it

numerically. Imposing the backward FDTD on Eq. (21) and using $\Delta\varphi(t,r,z) \rightarrow \Delta\varphi(i,j,k)$, it gives the following expression:

$$\Delta\phi(i,j,k) = \Delta\phi(i,j,k-1) + \frac{2\pi\Delta z}{\lambda_1}\{\Delta n^{o,\omega}[T(i,j,k)] + \Delta n^{e,\omega}[T(i,j,k)] - 2\Delta n^{e,2\omega}[T(i,j,k)]\}. \quad (22)$$

As Eq. (22) shows, to solve the TIPM, we need the temperature distribution, $T(i,j,k)$, first. Therefore, we initially solve the heat equation and then calculate the TIPM.

3. RESULTS AND DISCUSSION

In this work, Gaussian pulses with duration of $\tau_p = 50$ μs, wavelength of 532 nm, peak energy of 0.09 J, repetition rate of 500 Hz, and beam spot size of 100 μm were considered. In order to calculate a spatiotemporal-dependent temperature and TIPM for a KTP crystal under a repetitively pulsed pumping source, homemade codes with the FDTD method were developed. We have considered a cylindrical KTP crystal with a radius of $a = 5$ mm and a length of $l = 2$ cm [9]. The lateral surface of the crystal was assumed to be kept in a constant temperature of 298 K, whereas the beginning and end faces of the crystal are allowed to be cooled via convection and radiation as well [3,27]. The codes have been written in Intel Fortran 14.04 and run in Linux Ubuntu operating system. The meshes have been chosen such that stable and accurate solutions in a quickest time are achieved. The number of time steps for every pulse was chosen to be $N_t = 2532$. For radial and longitudinal directions, $N_r = 120$ and $N_z = 12000$ meshes were chosen, respectively. Under these conditions, the stability in solution was achieved and the program did not show any noticeable improvement in solutions with increasing the number of meshes. We tried to run the problem with home-used computing machines which are easily accessible.

Here it is worth explaining briefly the method of reducing required memory and run time for this problem. Overall, the temperature depends on five parameters: number of pulses, number of time steps, and three numbers standing for radial, azimuthal, and longitudinal coordinates' steps. With dropping the azimuth coordinate, the temperature should be a four dimensions array. If it is supposed that for each member of such array only one byte is needed, which is a quite underestimated rough number, we estimated that we need an 116 GB of RAM, which is not practically possible. In order to reduce the member of temperature array more, we omitted the index of number of pulses in our code. We changed the code to store only the data of the last pulse, which is itself quite arbitrary and depends on how many pulses are going to be reported. Therefore, we did not allow the code to keep all pulses' data in the RAM. This scheme reduced the number of array members by a factor of number of pulses. The next step to reduce the array's members, is discarding all time steps' data except that of ith time step, which is used for $(i+1)$th time step. With this idea, only the data of two successive time steps, i.e., i and $i+1$ are kept in the RAM. In conclusion, we reduced the required RAM volume by a factor of 5×10^9. With this idea, the run time for a microsecond pulse, which was already several hours, reduced to only 5 s.

As we are going to investigate the TIPM due to dn/dT effect (this effects dominates the bulging and stress birefringence effects [2]), and since this effect disturbs the wavefront, in Figs. 1(a) and 1(b) we illustrate qualitatively the curving of the phase plane of a wave for positive and negative sign dn/dT, respectively. For three waves interacting along the crystal, the sign of their corresponding dn/dT's differ depending on wavelength and temperature. Therefore, if the waves are matched in phase at $z = 0$ plane, they will lose the matching once they start traveling along the z-axis. As we will show in continue, the net result would be a negative mismatched phase due to temperature rise along the crystal axis.

The heat source given by Eq. (4) provides only one pulse, but we are interested in a repetitively pulsed pumping scheme. Therefore, to account for successive pulses, we follow an idea

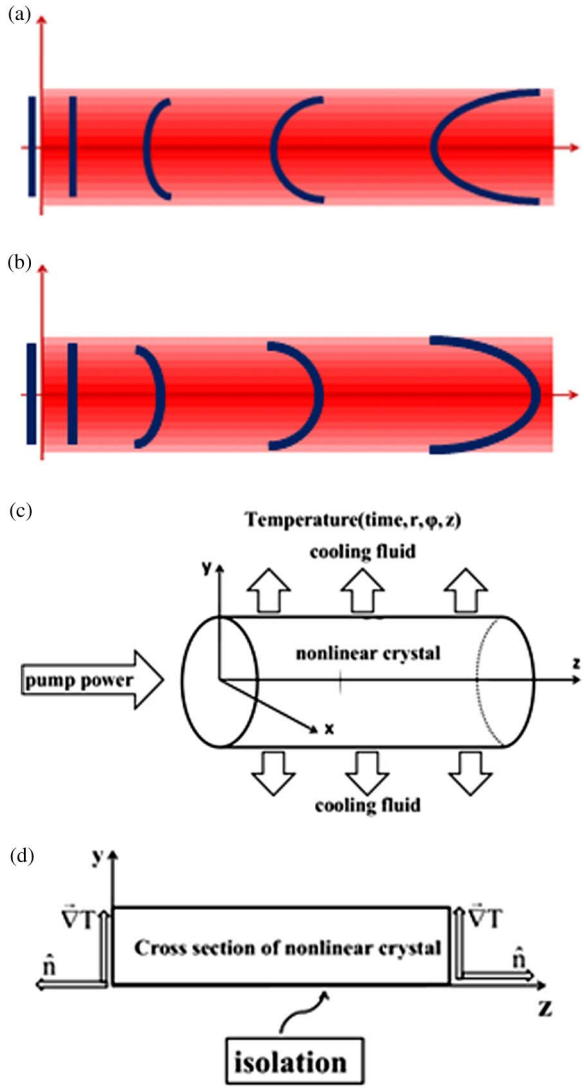

Fig. 1. Wavefront distortion due to (a) positive thermal dispersion ($dn/dT > 0$), and (b) negative thermal dispersion ($dn/dT < 0$). (c) A geometry of KTP crystal with direction of pumping and cooling. For lateral boundary, the condition of constant temperature (at $T = 298$ K) and for end faces, the conditions of convection and radiation conditions have been considered. (d) The rz-plane of KTP crystal.

as follows: the temperature of any point of the crystal at the latest time step was considered as an initial temperature of the next pulse at the same point. This procedure has been continued until all pulses were irradiated onto the crystal. Between two successive pulses, there is an off-time in which the crystal does not receive any noticeable heat energy, while it dissipates deposited heat energy through the conduction, convection, and radiation continuously, so that the temperature drops between two successive pulses.

Figure 1(c) represents the scheme of the crystal with direction of pumping, cooling mechanisms, and spatial coordinates. Assuming a cooling fluid flowing around the crystal, the crystal surface can be kept at a constant temperature. For two beginning and end faces of the crystal, the conditions of radiation and convection have been considered. We have shown already in our previous work [27] that for large crystal radius (≥5 mm) along with large pump beam spot (~3 mm) the heat radiation would be influential on the temperature of the crystal. Therefore, to obtain an accurate solution, in this work we consider the radiation beside the convection. Azimuthal symmetry of the crystal and pumping profile allows us to consider only a rz-plane, so that huge saving in RAM and time can be reached. Figure 1(d) shows a rz-plane along with numerical boundary conditions suitable for an actual problem. In the cylindrical coordinates, the $r = 0$ line must be assumed to be a thermal isolated line, i.e., $\partial T/\partial r = 0$ should be used at $r = 0$, because the heat flows from $r = 0$ line (which is the hottest line) toward $r = a$ (the coldest line) and no heat can cross $r = 0$ line.

Figure 2 shows the time evolution of the crystal temperature at $r = 0$ and $z = 0$ [Fig. 2(a)] and at $r = 0$ and $z = l$ [Fig. 2(b)] for two successive pulses with frequency of 500 Hz (i.e., an off-time of 0.02 s). This event is seen in Figs. 2(a) and 2(b). However, an accumulative behavior is seen for temperature, overall. In case the time-off between two successive pulses is shortened, i.e., if the repetition frequency is increased, the accumulative behavior gets strong and the crystal temperature reaches quickly the final temperature. On the other hand, as we have shown in our previous work devoted to interaction of a pulsed CO_2 laser with human tooth [43], if the repetition rate is lowered, temperature accumulation does not occur and pulses can be treated independently.

For TIPM, we have to show it at a plane other than $z = 0$ plane, since phase mismatching happens as a result of propagation of waves along the crystal axis. As one may expect, it grows as the waves travel more distance along the crystal axis. Figure 3 shows the TIPM at the central point of the end face of the crystal, i.e., at $r = 0$ and $z = l$. As this figure shows, the TIPM for KTP shows a behavior similar to temperature, but with a negative sign, which is a specific character of KTP with respect to its thermo-optical properties. For two successive pulses with pulse energy of 0.09 J, frequency of 500 Hz, and a beam spot size of 100 μm, a ~ – 45 rad TIPM for the first pulse and a ~ – 50 rad for the second pulse occurs.

The main question is that how much is the final value of TIPM and when it is saturated? At the first glance, it seems that the TIPM has an accumulative behavior with increasing the number of pulses. However, Figs. 4(a), 4(b), and 4(c), which have been prepared for 10, 100, and 5000 successive pulses, respectively, indicate that the TIPM approaches to a steady-state value. For $N_p = 100$ [Fig. 4(b)], the TIPM is near its steady state. For sure, we have continued increasing the number of irradiated pulses to $N_p = 5000$, shown in Fig. 4(c). A saturated behavior for large number of pulses is obvious in Fig. 4(c).

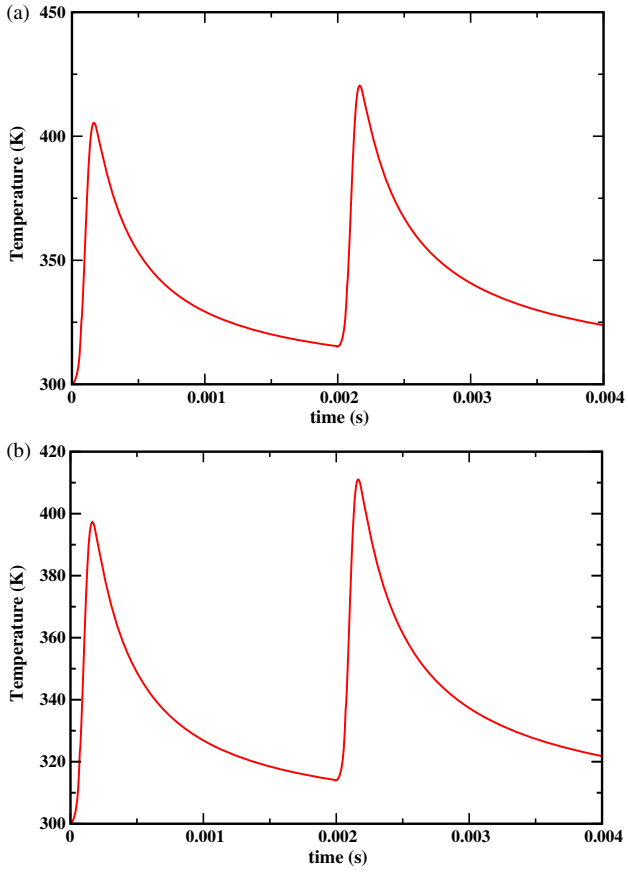

Fig. 2. Temporal variations of temperature at (a) $r = 0$ and $z = 0$ and, (b) $r = 0$ and $z = L$ for two pulses with frequency of $f = 500$ Hz.

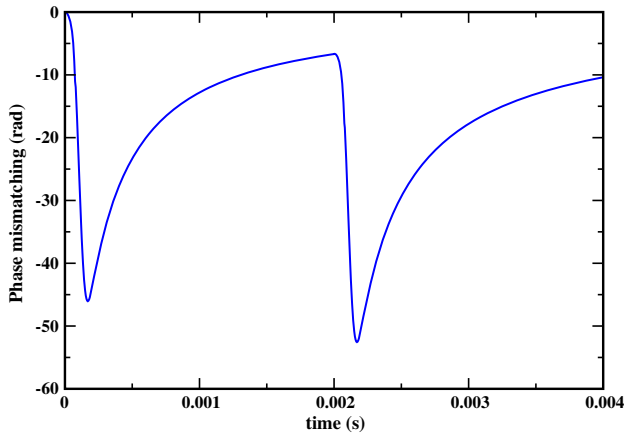

Fig. 3. Temporal variations of thermally induced phase mismatching (TIPM) at $r = 0$ and $z = L$ for two successive pulses with frequency of $f = 500$ Hz.

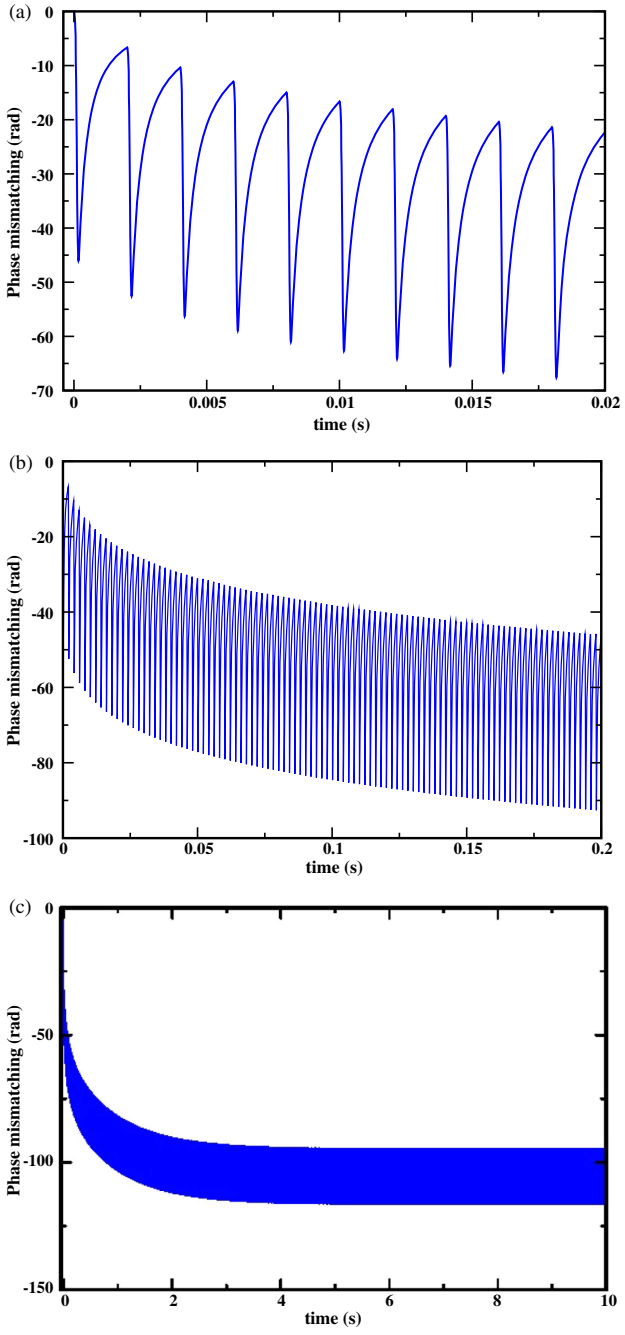

Fig. 4. TIPM as a function of time for (a) $N_p = 10$, (b) $N_p = 100$, and (c) $N_p = 5000$.

The fluctuations associated with the TIPM curves result from the off-time between two successive pulses. In fact, this behavior originates from the temperature behavior discussed earlier. At the steady state, the average heat energy flux inward the crystal accompanied with pulses, equals to the heat dissipated from the crystal surface through the conduction (lateral surface), convection (end and lateral surfaces), and radiation (end faces). As Sabaeian reported in his analytical work [36], where the radiation and the temperature dependence of thermal conductivity were ignored for sake of simplicity, with increasing the repetition rate of the pulses, the temperature fluctuations decrease and the curves go toward those corresponding to a CW heat source. For short pulses with a high enough repetition rate, the heat source power can be approximated with a continuous source as $P = fE$, where f is the repetition rate and E is the energy of each pulse.

The spatial distributions of temperature and TIPM along the radial distance for different number of pulses are shown in Fig. 5. For $N_p = 5000$, we are assured that the temperature reaches its steady state. The maximum temperature at the beginning face reaches ~490 K [Fig. 5(a)] and at the end face reaches ~465 K [Fig. 5(b)] for pulse specifications mentioned

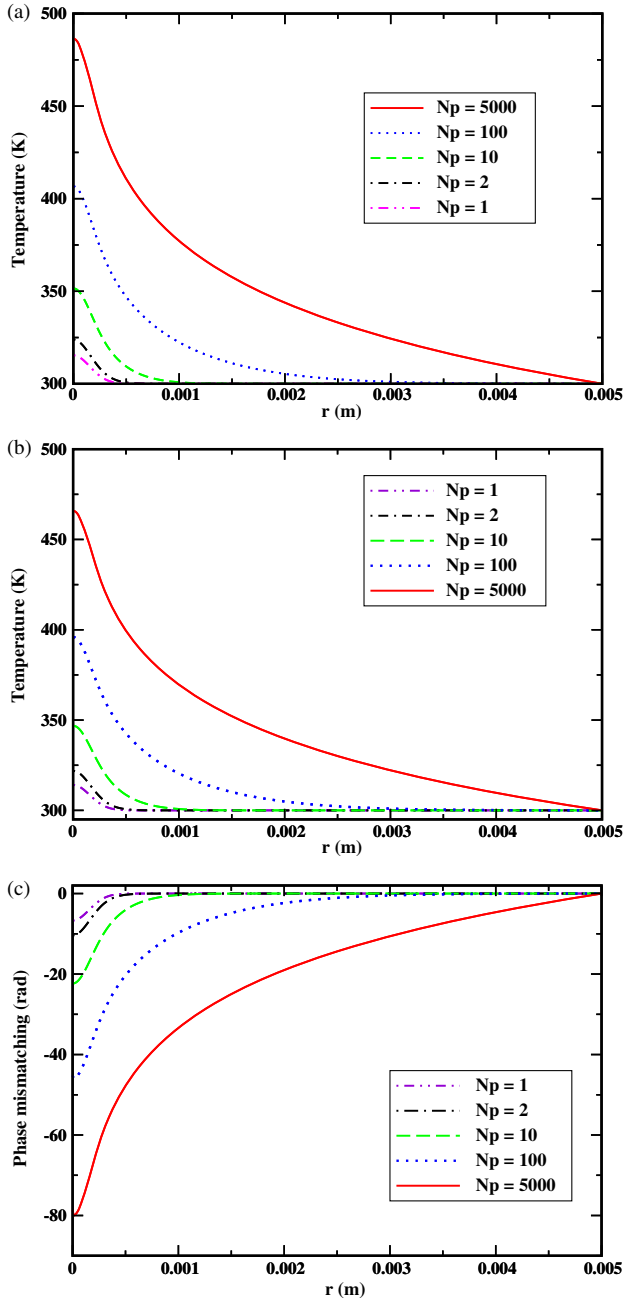

Fig. 5. Temperature distribution along the radial distance at (a) $z = 0$ and (b) $z = L$. (c) TIPM along the radial distance at $z = L$ for different number of pulses.

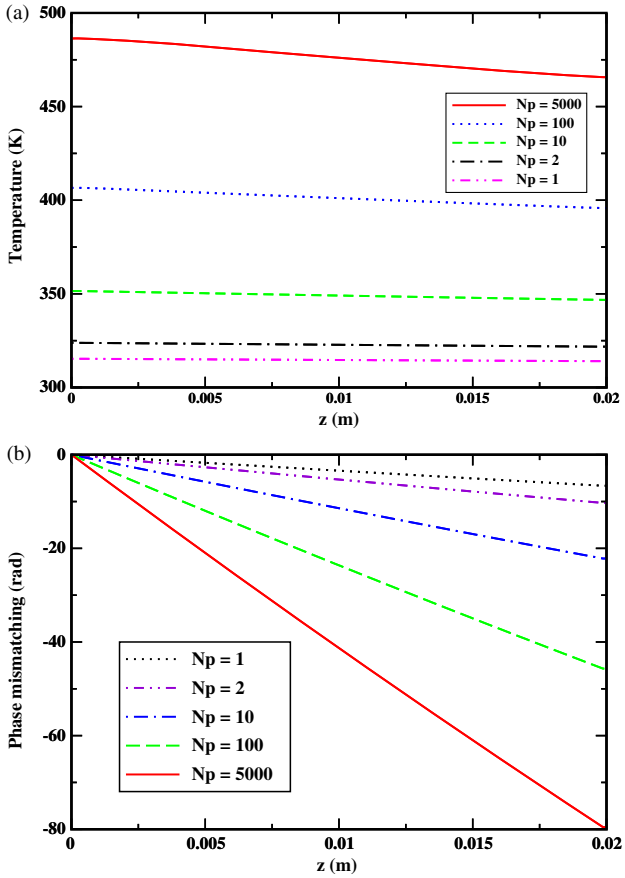

Fig. 6. Distribution of (a) temperature and (b) TIPM along the crystal axis for different number of pulses.

in previous figures. The corresponding TIPM at $z = l$ is about −80 rad [Fig. 5(c)]. This value vanishes at the crystal lateral surface where the crystal temperature equals to the ambient temperature.

To complete our discussion, we represent the temperature and TIPM along the crystal z-axis for various pulse numbers shot onto the crystal. Figure 6(a) shows the temperature along the crystal z-axis. Due to the overall low absorption coefficient of KTP at 523 nm, which is about 4 m^{-1}, the variations of temperature along the crystal axis are moderate. However, for TIPM, shown in Fig. 6(b), the scenario becomes different, because it is calculated through an integral over the longitudinal length. Therefore, even for a constant temperature along the crystal axis, TIPM increases (with its negative sign) along the crystal axis.

4. CONCLUSION

In conclusion, we have calculated the temperature and especially the TIPM in a KTP crystal due to optical absorption of the SHW when the crystal is under repetitively pulsed pumping. We have ignored the absorption of the fundamental wave since it is lower sufficiently than that of the SHW by 8 times (0.5 m^{-1} for 1064 nm and 4 m^{-1} for 532 nm [30]). The results were calculated for a pulsed SHW with energies of 0.09 J and beam spot size of 100 μm. Accumulative behaviors for temperature and TIPM were seen with increasing the number of pulses. It was shown that both temperature and TIPM approach finally to their steady states accompanied with some fluctuations. For TIPM, negative values were achieved for positive temperature changes that return back to the thermo-optical properties of the KTP. This work can provide a good insight to the problem of reducing nonlinear conversion efficiency in nonlinear lasers.

M. M. Rezaee, M. Sabaeian, A. Motazedian, and F. S. Jalil-Abadi would like to thank Shahid Chamran University of Ahvaz for supporting this work.

REFERENCES

1. J. A. Armstrong, N. Bloembergen, J. Ducuing, and P. S. Pershan, "Interactions between light waves in a nonlinear dielectric," Phys. Rev. **127**, 1918–1939 (1962).
2. M. Sabaeian, F. S. Jalil-Abadi, M. M. Rezaee, and A. Motazedian, "Heat coupled Gaussian continuous-wave double-pass type-II second harmonic generation: inclusion of thermally induced phase mismatching and thermal lensing," Opt. Express **22**, 25615–25628 (2014).
3. M. Sabaeian, L. Mousave, and H. Nadgaran, "Investigation of thermally-induced phase mismatching in continuous-wave second harmonic generation: A theoretical model," Opt. Express **18**, 18732–18743 (2010).
4. C. A. Klein, "Oxyfluoride glass for high-energy laser windows: Thermal lensing issue," Appl. Phys. Lett. **87**, 231117 (2005).
5. C. A. Klein, "Optical distortion coefficients of high-power laser windows," Opt. Eng. **29**, 343–350 (1990).
6. A. Sayahian Jahromi, M. Sabaeian, and H. Nadgaran, "Heat coupled laser rate equations: A model for Er-doped fiber lasers," Opt. Commun. **311**, 134–139 (2013).
7. T. Harimoto, B. Yo, and K. Uchida, "Compensation for the thermal effect in the second-harmonic generation of a Q-switched nanosecond-kilohertz Nd: YVO4 laser," Opt. Rev. **19**, 341–344 (2012).
8. S. Kumar, S. Sabouri, A. Khorsandi, and M. Ebrahim-Zadeh, "Thermal effects in high-power continuous-wave single-pass second harmonic generation," IEEE J. Sel. Top. Quantum Electron. **20**, 7500210 (2014).
9. S. Seidel and G. Mann, "Numerical modeling of thermal effects in nonlinear crystals for high-average-power second harmonic generation," Proc. SPIE **2989**, 204–214 (1997).
10. H. Nadgaran, M. Servatkhah, and M. Sabaeian, "Mathieu–Gauss beams: A thermal consideration," Opt. Commun. **283**, 417–426 (2010).
11. M. Sabaeian and H. Nadgaran, "Bessel–Gauss beams: Investigations of thermal effects on their generation," Opt. Commun. **281**, 672–678 (2008).
12. H. Nadgaran and M. Servatkhah, "The effects of induced heat loads on the propagation of Ince–Gaussian beams," Opt. Commun. **284**, 5329–5337 (2011).
13. M. Sabaeian, "The effects of air-holes on temperature and temperature gradient of solid-core photonic crystal fiber lasers," Optik **124**, 5787–5791 (2013).
14. L. Mousavi, M. Sabaeian, and H. Nadgaran, "Thermally-induced birefringence in solid-core photonic crystal fiber lasers," Opt. Commun. **300**, 69–76 (2013).
15. H. Zhang, S. Virally, Q. Bao, L. Kian Ping, S. Massar, N. Godbout, and P. Kockaert, "Z-scan measurement of the nonlinear refractive index of graphene," Opt. Lett. **37**, 1856–1858 (2012).
16. Z. Sun, T. Hasan, F. Torrisi, D. Popa, G. Privitera, F. Wang, F. Bonaccorso, D. M. Basco, and A. C. Ferrari, "Graphene mode-locked ultrafast laser," ACS Nano **4**, 803–810 (2010).
17. P. Li, G. Zhang, H. Zhang, C. Zhao, J. Chi, Z. Zhao, C. Yang, H. Hu, and Y. Yao, "Q-switched mode-locked Nd: YVO4 Laser by topological insulator Bi2Te3 saturable absorber," IEEE Photon. Technol. Lett. **26**, 1912–1915 (2014).

18. M. Liu, X.-W. Zheng, Y.-L. Qi, H. Liu, A.-P. Luo, Z.-C. Luo, W.-C. Xu, C.-J. Zhao, and H. Xhang, "Microfiber-based few-layer MoS2 saturable absorber for 2.5 GHz passively harmonic mode-locked fiber laser," Opt. Express **22**, 22841–22846 (2014).
19. Z. Zheng, C. Zhao, S. Lu, Y. Chen, Y. Li, H. Zhang, and S. Wen, "Microwave and optical saturable absorption in graphene," Opt. Express **20**, 23201–23214 (2012).
20. J. J. Dean and H. M. van Driel, "Second harmonic generation from graphene and graphitic films," Appl. Phys. Lett. **95**, 261910 (2009).
21. Y. Li, Y. Rao, K. F. Mak, Y. You, S. Wang, C. R. Dean, and T. F. Heinz, "Probing symmetry properties of few-layer MoS2 and h-BN by optical second-harmonic generation," Nano Lett. **13**, 3329–3333 (2013).
22. L. M. Malard, T. V. Alencar, A. P. M. Barboza, K. F. Mak, and A. M. de Paula, "Observation of intense second harmonic generation from MoS2 atomic crystals," Phys. Rev. B **87**, 201401 (2013).
23. A. A. Balandin, "Thermal properties of graphene and nanostructured carbon materials," Nat. Mater. **10**, 569–581 (2011).
24. A. A. Balandin, S. Ghosh, W. Bao, I. Calizo, D. Teweldebrhan, F. Miao, and C. N. Lau, "Superior thermal conductivity of single-layer graphene," Nano Lett. **8**, 902–907 (2008).
25. S. Lepri, R. Livi, and A. Politi, "Thermal conduction in classical low-dimensional lattices," Phys. Rep. **377**, 1–80 (2003).
26. K. Regelskis, J. Želudevičius, N. Gavrilin, and G. Račiukaitis, "Efficient second-harmonic generation of a broadband radiation by control of the temperature distribution along a nonlinear crystal," Opt. Express **20**, 28544–28556 (2012).
27. M. M. Rezaee, M. Sabaeian, A. Motazedian, F. S. Jalil-Abadi, and A. Khaledi-Nasab, "Complete anisotropic time-dependent heat equation in KTP crystal under repetitively pulsed Gaussian beams: A numerical approach," Appl. Opt. **54**, 1241–1249 (2015).
28. M. Sabaeian, F. S. Jalil-Abadi, M. M. Rezaee, and A. Motazedian, "Temperature distribution in a Gaussian end-pumped nonlinear KTP crystal: the temperature dependence of thermal conductivity and radiation boundary condition," Braz. J. Phys. **45**, 1–9 (2015).
29. M. Sabaeian, A. Motazedian, M. M. Rezaee, and F. S. Jalil-Abadi, "Bessel-Gauss beams: pulsed Bessel-Gauss beams: a depleted wave model for type II second harmonic generation," Appl. Opt. **53**, 7691–7696 (2014).
30. D. Nikogosyan, *Nonlinear Optical Crystals: A Complete Survey: A Complete Survey* (Springer, 2006).
31. Z.-C. Tan, G.-Y. Sun, Y.-J. Song, L. Wang, J.-R. Han, Y.-S. Liu, M. Wang, and D.-Z. Nie, "An adiabatic calorimeter for heat capacity measurements of small samples: The heat capacity of nonlinear optical materials KTiOPO4 and RbTiOAsO4 crystals," Thermochim. Acta **352–353**, 247–253 (2000).
32. C. Pfistner, R. Weber, H. P. Weber, S. Merazzi, and R. Gruber, "Thermal beam distortions in end-pumped Nd:YAG, Nd:GSGG, and Nd:YLF rods," IEEE J. Quantum Electron. **30**, 1605–1615 (1994).
33. H. Glur, R. Lavi, and T. Graf, "Reduction of thermally induced lenses in Nd:YAG with low temperatures," IEEE J. Quantum Electron. **40**, 499–504 (2004).
34. C. K. Ong, E. H. Sin, and H. S. Tan, "Heat-flow calculation of pulsed excimer ultraviolet laser's melting of amorphous and crystalline silicon surfaces," J. Opt. Soc. Am. B **3**, 812–814 (1986).
35. J. D. Bierlein and H. Vanherzeele, "Potassium titanyl phosphate: properties and new applications," J. Opt. Soc. Am. B **6**, 622–633 (1989).
36. M. Sabaeian, "Analytical solutions for anisotropic time-dependent heat equations with Robin boundary condition for cubic-shaped solid-state laser crystals," Appl. Opt. **51**, 7150–7159 (2012).
37. M. Sabaeian, H. Nadgaran, and L. Mousave, "Analytical solution of the heat equation in a longitudinally pumped cubic solid-state laser," Appl. Opt. **47**, 2317–2325 (2008).
38. J. Arlt, V. Garces-Chavez, W. Sibbett, and K. Dholakia, "Optical micromanipulation using a Bessel light beam," Opt. Commun. **197**, 239–245 (2001).
39. K. Kato, "Parametric oscillation at 3.2 μm in KTP pumped at 1.064 μm," IEEE J. Quantum Electron. **27**, 1137–1140 (1991).
40. Y. Bi, R. Li, Y. Feng, X. Lin, D. Cui, and Z. Xu, "Walk-off compensation of second harmonic generation in type-II phase-matched configuration with controlled temperature," Opt. Commun. **218**, 183–187 (2003).
41. R. W. Boyd, *Nonlinear Optics* (Academic Press, 2003).
42. K. Asaumi, "Second-harmonic power of KTiOPO4 with double refraction," Appl. Phys. B **54**, 265–270 (1992).
43. M. Sabaeian and M. Shahzadeh, "Simulation of temperature and thermally induced stress of human tooth under CO2 pulsed laser beams using finite element method," Lasers Med. Sci. **30**, 645–651 (2015).